Potent LILRB1 D1D2-containing antibodies inhibit RIFIN-mediated immune evasions

Yizhuo Wang[1,2,#], Hengfang Tang[1,#], Wanxue Wang[2,3], Ming Li[2], Chenchen Zhu[1,2], Han Dai[1], Hongxin Zhao[1,4,*], Bo Wu[2,*], Junfeng Wang[1,2,*]

[1]High Magnetic Field Laboratory, Key Laboratory of High Magnetic Field and Ion Beam Physical Biology, Hefei Institutes of Physical Science, Chinese Academy of Sciences, Hefei, Anhui 230031, China.

[2]University of Science and Technology of China, Hefei, Anhui 230026, China.

[3]Department of Anatomy, School of Basic Medical Sciences, Anhui Medical University, Hefei, China.

[4]Hefei China Science Longwood Biological Technology Co., Ltd. Hefei, Anhui 230088, China.

[#] Those authors contributed equally.

*Corresponding authors. Email: zhx@hmfl.ac.cn (Hongxin Zhao), wubo@hmfl.ac.cn (Bo Wu), junfeng@hmfl.ac.cn (Junfeng Wang).

Abstract

The spread of drug-resistant malaria parasites presents a major challenge to global efforts in malaria control, increasing the urgency for new treatments and vaccines. A promising approach involves developing antibodies that can counteract the parasite's immune evasion mechanisms. In this study, we designed a receptor-containing antibody, targeting the D1D2 domain of the LILRB1 receptor, using a structure-based rational approach. We began with the MDB1 antibody as a scaffold and replaced the LILRB1-D3D4 insertion domain with D1D2.v, a high-affinity variant optimized through yeast surface display. The modified D1D2.v-IgG efficiently blocked the interaction between RIFIN#1 (from PF3D7_1254800) and LILRB1, thereby reversing the inhibition of NK cell activity caused by RIFIN#1. To further enhance this effect, we developed NK-biAb, a bispecific antibody based on D1D2.v-IgG that targets both RIFIN#1 and NKG2D receptors. NK-biAb exhibited superior biological performance compared to D1D2.v-IgG alone. These findings provide a clear framework for designing antibodies that target immune evasion in malaria, potentially guiding the development of more effective treatments and vaccines.

Keywords: *Plasmodium falciparum*, immune evasion, RIFIN, receptor-containing antibody

41 **Introduction**

42 Malaria remains one of the deadliest infectious diseases globally, with
43 Plasmodium falciparum being the species most responsible for high mortality rates,
44 particularly in sub-Saharan Africa[1,2]. The emergence and spread of drug-resistant P.
45 falciparum strains pose a significant threat to current malaria control efforts,
46 underscoring the urgent need for new treatments and vaccines[3-5]. The life cycle
47 of Plasmodium falciparum is complex, spanning several developmental stages between
48 the mosquito vector and the human host. Among these, the blood stage is primarily
49 responsible for the clinical symptoms of malaria, including fever and anemia[6,7]. During
50 this stage, P. falciparum invades erythrocytes, where it replicates and displays a variety
51 of variable surface antigens on infected erythrocytes (IEs). These blood-stage parasites
52 are the primary target of acquired immunity. However, by interacting with host immune
53 receptors, these surface antigens allow P. falciparum to evade immune detection,
54 contributing to the slow development of naturally acquired immunity against malaria[7].

55 RIFINs, the largest family of surface antigens expressed by P. falciparum, are key
56 players in immune evasion[7,8]. These antigens include numerous isoforms, each capable
57 of binding to different domains of host receptors such as LAIR1 or LILRB1[9-12] (Fig.
58 1a). For instance, RIFIN PF3D7_1254800 binds preferentially to the D1D2 domain of
59 LILRB1[9], while RIFIN PF3D7_1101100 interacts with LAIR1 rather than LILRB1[10].
60 Blocking these receptor-RIFIN interactions could prevent immune evasion and enhance
61 immune clearance, providing a potential strategy for developing effective malaria
62 treatments and vaccines[13,14].

63 Recent studies have identified several receptor-based antibodies containing
64 LAIR1 and LILRB1-D3D4 fragments designed to target these immune evasion
65 mechanisms[15-17] (Fig. 1b). Unlike conventional antibodies, which bind antigens through
66 their variable regions, these receptor-containing antibodies incorporate LAIR1 or
67 LILRB1 fragments between the variable and constant regions of the heavy chain,
68 enabling them to directly target specific RIFIN antigens. LAIR1-containing antibodies,

69 in particular, have undergone specific mutations that enhance their affinity for RIFINs[16].
70 In contrast, LILRB1-containing antibodies retain the unmutated LILRB1-D3D4
71 domain or just the D3 domain in the variable-constant (VH-CH1) elbow region[15] (Fig.
72 1c). Although some RIFINs bind to the LILRB1-D1D2 domain, mimicking the
73 interaction of β2-microglobulin with MHC class I molecules, no antibodies targeting
74 this domain have been identified. This may be due to the inherently low affinity
75 between RIFINs and LILRB1-D1D2. Moreover, developing receptor-containing
76 antibodies in vivo is time-consuming, particularly due to the uncontrollable nature of
77 the affinity maturation process.

78 In this study, we introduce a rational, structure-based approach to design a
79 receptor-containing antibody that targets the D1D2 domain of LILRB1. This newly
80 developed antibody family mimics the natural immune recognition mechanism,
81 providing a novel strategy to competitively inhibit RIFIN-mediated immune evasion.
82 To create a high-affinity D1D2 variant (D1D2.v) capable of antagonizing the
83 interaction between LILRB1 and RIFIN#1 (from PF3D7_1254800), we used yeast
84 surface display to direct the evolution of the LILRB1-D1D2 domain[18-20]. The receptor-
85 containing antibody MDB1 served as the scaffold, and we replaced the LILRB1-D3D4
86 insertion domain with D1D2.v to generate the D1D2.v-containing antibody, D1D2.v-
87 IgG (Fig. 1d). This newly engineered antibody demonstrated a 110-fold higher affinity
88 for RIFIN#1 than the native LILRB1-D1D2 domain, successfully blocking the
89 interaction and restoring NK cell activity suppressed by RIFIN#1. Building on this
90 success, we further developed a bispecific antibody, NK-biAb, based on D1D2.v-IgG,
91 which includes an NKG2D-specific scFv (KYK2.0) at its C-terminus[21-23]. This design
92 aims to redirect NK cells toward parasite-infected erythrocytes, mimicking CAR-NK
93 therapy[24,25]. NK-biAb showed superior biological activity in enhancing NK cell-
94 mediated cytotoxicity compared to D1D2.v-IgG alone. These findings establish a
95 framework for the development of novel antibodies targeting immune evasion
96 mechanisms, providing new avenues for malaria treatment and vaccine development.

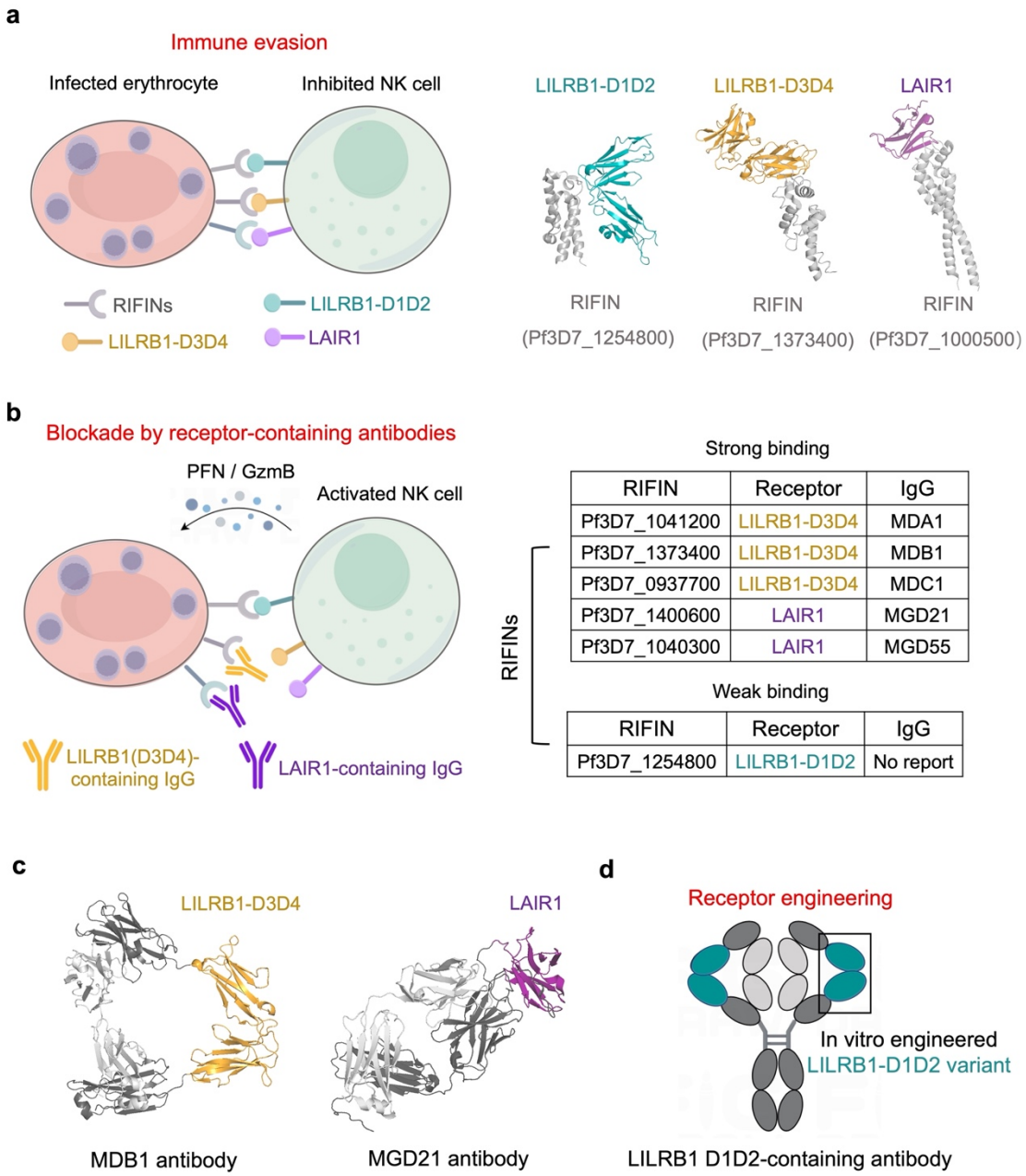

Figure. 1: Immune evasion of *P.falciparum* and design of novel receptor-containing antibody (**a**) Mechanisms of immune evasion of *P. falciparum* and structures of RIFIN and immunoinhibitory receptors**.** Different RIFIN isoforms bind to their corresponding receptor domains and transduce immunosuppressive signals (PDB: 6ZDX, 7KFK and 7F9N). (**b**) Receptor-containing antibodies in inhibiting immune evasion of *P. falciparum* and identification of LILRB1- and LAIR1-containing antibodies. All reported LILRB1-containing antibodies only have LILRB1-D3D4 domains and no antibodies that contain LILRB1-D1D2 domains were found. (**c**) Two representative receptor-containing antibody. The left one is LILRB1 D3D4-containing antibody MDB1 (PDB:7KHF) and the right one is LAIR1-containing antibody MGD21 (PDB: 7JZ4). (**d**) Strategy for generating high-affinity LILRB1 D1D2-containing antibodies. The affinity-matured LILRB1-D1D2 variant was

generated through structure-based affinity maturation in vitro and then the LILRB1-D1D2 variant was grafted into the framework of MDB1 by replacing LILRB1-D3D4 domains.

Results

Structure-guided engineering of a high affinity LILRB1 D1D2 variant

RIFIN#1 binds to the extracellular domain (ECD) of LILRB1 through its variable region with a moderate affinity (K_d =570 ± 130 nM). LILRB1-ECD comprises four immunoglobulin-like domains (D1-D4), and its complex structure with RIFIN#1 suggests that the interaction is mediated by the D1D2 domain[9]. In order to obtain a high-affinity variant capable of competitively antagonizing LILRB1-RIFIN#1 interaction, we performed structure-guided directed evolution of the LILRB1-D1D2 domain by yeast surface display. A library of LILRB1 D1D2 mutations was designed using the structure of the LILRB1-RIFIN#1 complex as a guide. As shown in Figure 2a, ten LILRB1 D1D2 residues (K42, E68, G97, A98, Y99, I100, Q125, V126, F128, E184) interfacing with RIFIN#1 were altered based on the structural information by randomized PCR. The resulting D1D2 mutant library contained $2x10^7$ transformants. The library was then displayed on the yeast surface, stained with biotinylated RIFIN , and screened to isolate high-affinity binders (Fig. 2b and Fig. S1). In total, eight round of sorting were performed (Fig. S2). Three rounds of sorting with decreasing concentrations of biotinylated RIFIN tetramers (2 μM, 1 μM and 0.3 μM) (Fig. S3) and three rounds of sorting with decreasing concentrations of biotinylated RIFIN monomers (0.3 μM, 0.1μM and 0.02 μM) (Fig. S4) were performed for binder enrichment. For kinetic sorting, enriched library was screened using 0.02 μM biotinylated RIFIN monomers in the presence of approximately a 50-fold excess unlabeled competition RIFIN, with a duration of 2 h and 4 h respectively (Fig. S5). After completion of all eight rounds of sorting, yeast cells were transplanted to obtain individual clones. DNA sequencing results indicate that a single D1D2 mutant clone (named D1D2.v) dominates this enrichment process, and this consensus variant contains a total of nine

mutations: K42M, G97S, A98T, Y99F, I100T, Q125E, V126I, F128Q, E184H (Fig. 2c and Fig. S6).

To gain insight into the mechanisms of D1D2.v affinity enhancement, we obtained a structural model of D1D2.v binding to RIFIN#1 using SWISS-MODEL (Fig. 2d). Comparative analysis with the crystal structure of the LILRB1-RIFIN#1 complex show that D1D2.v binds to RIFIN#1 in essentially the same manner as its wild-type counterpart; however, some differences are observed at the binding interface. As shown in Figure 2d, the Q125E mutation establishes a new salt bridge with R233 on RIFIN#1. In addition, the G97S, A98T, and I100T mutations appears to enhance the strength of their H-bonds with RIFIN#1 based on analysis of the H-bond distance.

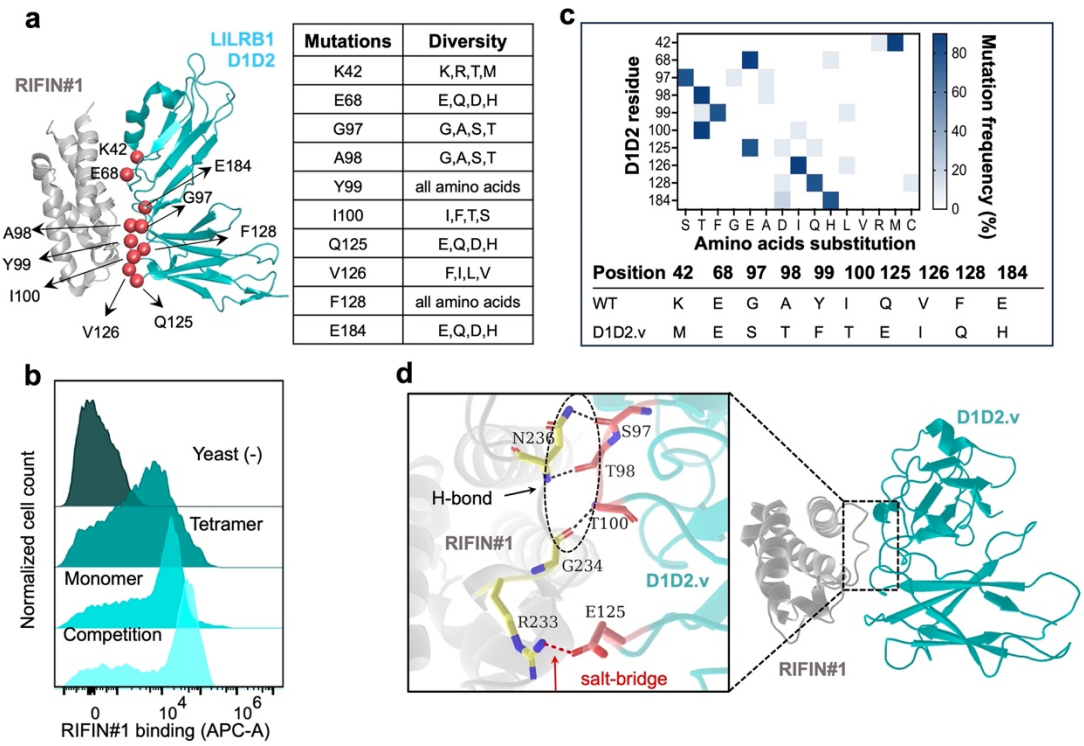

Figure. 2: Yeast display and affinity maturation of D1D2 domain

(**a**) (Left) LILRB1 models based on LILRB1-RIFIN#1 complex structure (PDB:6ZDX), where RIFIN#1 is in orange color, LILRB1-D1D2 is in cyan color, and the randomized positions are depicted by red balls; (Right) Table of random positions of the LILRB1-D1D2 interface library with possible amino acid variants. (**b**) Flow cytometry results for the yeast stained with biotinylated RIFIN#1 in tetramer, monomer and competition selection strategy. (**c**) Mutation frequencies (Above) and consensus D1D2.v sequence (Below). (**d**) Structural modeling and interface analysis. The sequences of D1D2.v and RIFIN#1 were imported into the SWISS-MODEL server for initial model generation based on the coordinates of PDB code**.** The G97S, A98T, I100T and Q125E mutations

155 in D1D2.v increases H-bonding strength targeting RIFIN#1, while a salt-bridge forms between
156 E125 on D1D2.v and R233 on RIFIN#1.
157

158 **Design and biochemical characterization of a D1D2.v-containing antibody that**
159 **antagonizes RIFIN#1-LILRB1 interaction.**

160 Recently, several natural LILRB1-containing monoclonal antibodies were
161 identified in malaria-infected individuals, such as MDB1, in which the LILRB1 D3D4
162 structural domain was inserted into its variable-conatant(VH-CH1) elbow region[15,16].
163 We then replaced the LILRB1-D3D4 insertion domain in MDB1 with D1D2.v to
164 generate a D1D2-containing antibody, named D1D2.v-IgG (Fig. 3a). To express as the
165 secreted protein, the codon-optimized antibody sequence was genetically linked to a N-
166 terminal Trp2 signal peptide sequence within a pTT5 expression vector. The
167 recombinant antibody was transiently expressed in Expi293F cells and purified from
168 culture supernatant by protein A affinity chromatography. The purity was confirmed by
169 SDS-PAGE analysis under both non-reducing and reducing conditions. To evaluate the
170 RIFIN#1-binding activity of this recombinant antibody, we generated the Fab fragment
171 by enzymatically removing the Fc tag and detected its binding with RIFIN#1 by size-
172 exclusion chromatography (SEC) assay. The results showed that Fab bound strongly to
173 RIFIN#1, forming a tight complex (Figure 3b). Next, we quantified the binding affinity
174 of D1D2.v-IgG to RIFIN#1 using a protein-based ELISA assay with purified LILRB1
175 ECD as a control. As shown in Fig. 3c, the dissociation constant (K_d) for LILRB1 ECD
176 binding to RIFIN#1 was approximately 650 nM, which is consistent with the previously
177 reported affinity determined using surface plasmon resonance (SPR). In contrast, the
178 affinity of D1D2.v-IgG binding to RIFIN#1 was significantly higher, with a K_d of 6
179 nM, a 110-fold increase (Fig. 3c). To assess the ability of D1D2.v-IgG to antagonize
180 the binding of LILRB1 to RIFIN#1, we performed a competitive ELISA assay. The
181 results showed that D1D2.v-IgG effectively inhibited the binding of LILRB1 to
182 RIFIN#1 in a dose-dependent manner with a half-maximal inhibitory concentration
183 (IC_{50}) of 20 nM (Fig. 3d).

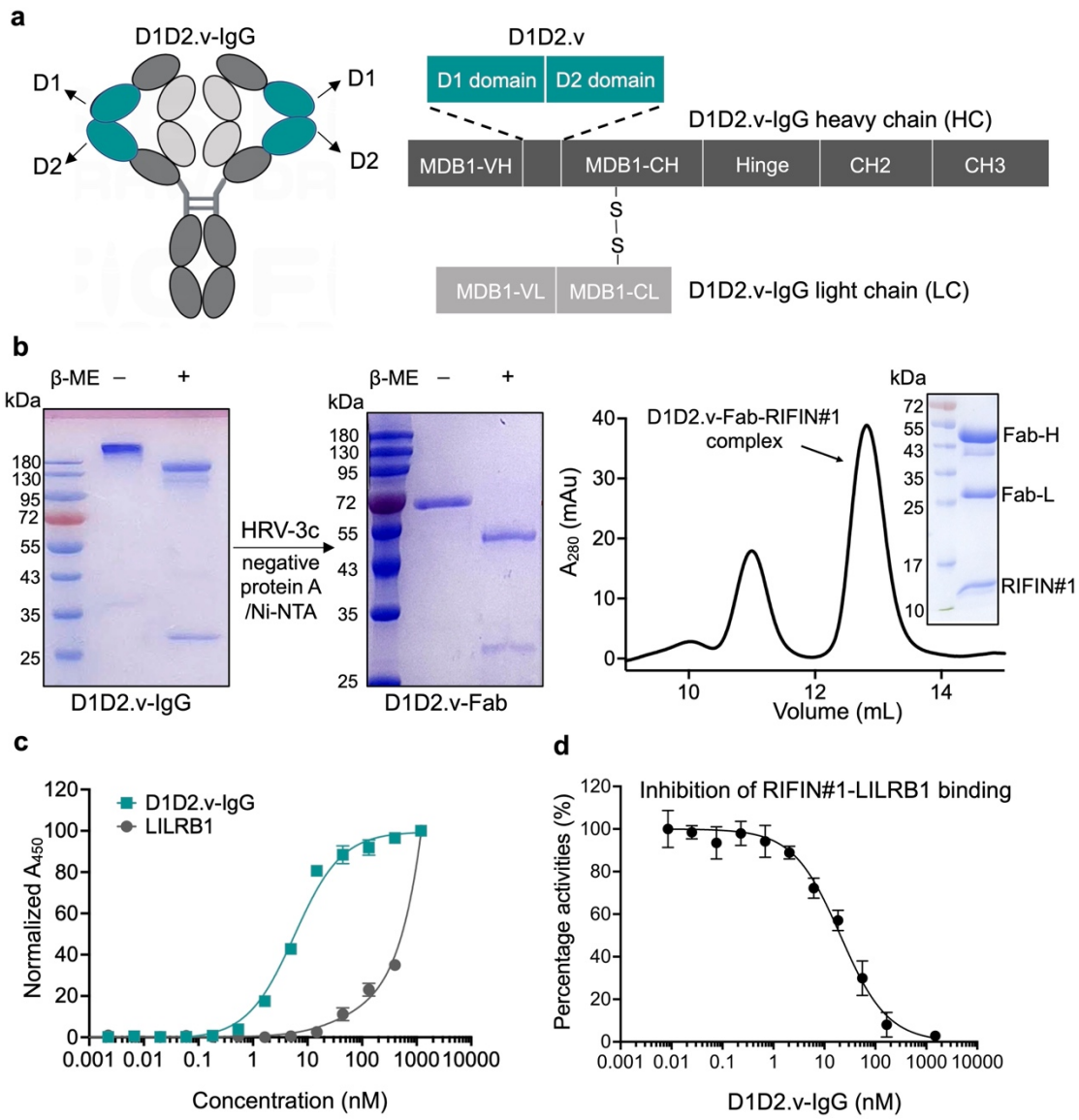

Fig. 3: Molecular design and biochemical characterization of the D1D2.v-IgG

(a) Molecular structure and cDNA frame of LILRB1 D1D2-containing IgG. The inserted LILRB1-D1 domain is colored in dark blue and LILRB1-D2 domain is colored in light blue, which are located between heavy variable chain (VH) and heavy constant chain (CH). The antibody heavy chain and Fc domain are depicted in dark grey and the light chain is depicted in light grey. **(b)** Purification and functional validation of the antigen binding fragment (Fab) of D1D2.v-IgG. SDS-PAGE (Left) show the purity and molecular weight of D1D2.v-IgG before protease digestion. SDS-PAGE (Right) show the purity and molecular weight of D1D2.v-Fab. Size-exclusion chromatography (SEC) chromatograms show the homogeneous Fab-RIFIN complex have a UV_{280} absorbance at around 13 mL. **(c)** Titration curves of wild-type LILRB1 (ECD) (dark green) and D1D2.v-IgG (red) binding to RIFIN in ELISA assay. Data are mean ± SD. **(d)** The representative competition binding curve using wild type LILRB1 (ECD) show D1D2.v-IgG antagonizes the RIFIN-LILRB1 (ECD) interaction effectively. Data represent mean ± SD of three technical replicates.

D1D2.v-IgG significantly enhances NK92 cytolytic activity against RIFIN#1-expressing K562 cells in vitro

Given that RIFIN#1 binding to LILRB1 inhibits NK cell responses, we subsequently investigated whether D1D2.v-IgG could enhance NK cell-mediated cytotoxicity by blocking the interaction between LILRB1 and RIFIN#1. To assess this, we performed NK92 cell cytotoxicity assays on K562 cells stably transfected with full length RIFIN#1 (Fig. S7). Flow cytometry verified the expression level of LILRB1 on NK92 cells (Fig. 4a). The RIFIN#1-expressing K562 cells were co-cultured with NK92 cells at two different effector to target (E: T) ratios of 2.5 and 12.5 in the presence or absence of D1D2.v-IgG. Flow cytometry analysis confirmed the specific binding of purified D1D2.v-IgG to the RIFIN#1-expresssing K562 cells (Fig. 4b). The cytotoxicity against K562 cells expressing RIFIN#1 was 5.8% in the absence of D1D2.v-IgG when the E:T ratio was 2.5, and increased significantly to 13.8% when D1D2.v-IgG at a concentration of 100 nM was added. Similarly, when the E:T ratio was 12.5, the cell killing efficiency was 35% in the absence of D1D2.v-IgG, but increased significantly to 61% when D1D2.v-IgG at a concentration of 100 nM was added (Fig. 4c). In addition, we observed that D1D2.v-IgG significantly increased the secretion of perforin and granzyme B from NK92 cells (Fig. 3d-e). These findings clearly indicate that D1D2.v-IgG can effectively stimulate NK-cell cytotoxicity against RIFIN#1-expressing K562 cells.

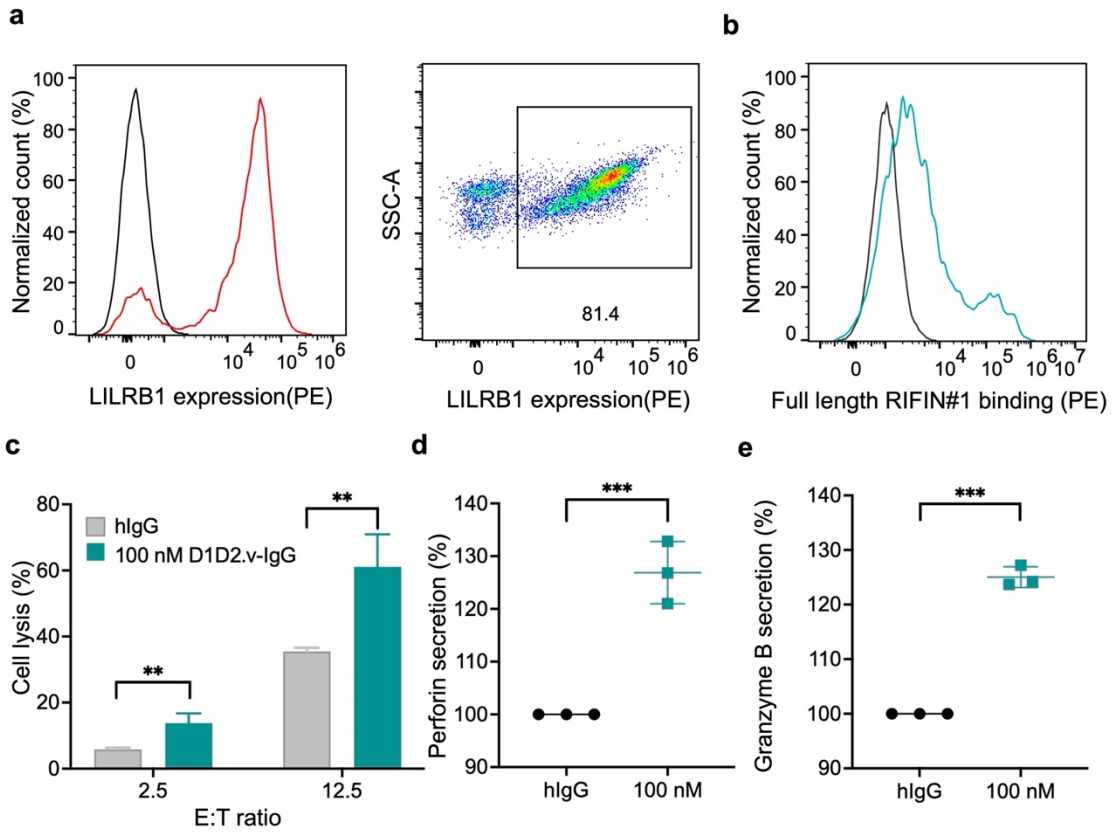

Fig. 4: D1D2.v-IgG enhanced NK cell cytotoxicity against RIFIN-expressing K562 cell

(**a**) Detection of the LILRB1 on NK92 cells by flow cytometry. The red curve shows the binding of LILRB1 antibody to LILRB1 on NK92 cells, while the blue curve informs the control sample of NK92 cells. (**b**) Detection of the purified D1D2.v-IgG bound to RIFIN#1-expressing K562 cells by flow cytometry. The red curve shows the binding of D1D2.v-IgG to full-length RIFIN#1 on stably-transfected K562 cells, while the cyan curve informs the blank sample of K562 cells. **(c)** The results for the NK92 cytotoxicity in the presence or absence of D1D2.v-IgG. RIFIN#1-expressing K562 cells were cocultured with NK92 cells and incubated with 100 nM control human IgG (hIgG) (Grey, n = 3) or 100 nM D1D2.v-IgG (Yellow, n = 3). (**d,e**) Detections of the perforin (e) and granzyme B (f) releases in the presence or absence of D1D2.v-IgG. RIFIN#1-expressing K562 cells were cocultured with NK92 cells (E: T ratio = 1: 1) and incubated with 100 nM control hIgG (Grey, n = 3) or 100 nM D1D2.v-IgG (Orange, n = 3). After the incubation for 24h, the perforin and granzyme B levels were determined by ELISA. Statistical test was t test and statistical significance was analyzed between D1D2.v-IgG and hIgG. *P<0.05; **P<0.01; ***P<0.001; ****P<0.0001.

Generation of a bispecific antibody targeting RIFIN#1 and NKG2D

Next, we developed a bispecific antibody that recruits NK cells to RIFIN#1-expressing cells using the D1D2.v-IgG as a basis. The redirection of NK cells requires a highly specific and high-affinity 'compass' (Fig. 5a). To fulfill this requirement, we chosen an engineered scFv called KYK2.0, which exhibits a nanomolar affinity towards

241 NKG2D expressed on all types of NK cells. By fusing the scFv form of KYK2.0 to the
242 C terminal of the Fc fragment of D1D2.v-IgG via a flexible GS linker, we generated a
243 bispecific antibody (bsAb), named NK-biAb (Fig. 5b). The resulting bsAb was then
244 transiently expressed and purified from Expi293F cell culture supernatants by affinity
245 chromatography. Integrity and purity of NK-biAb were analyzed by SDS-PAGE under
246 reducing and non-reducing conditions (Fig. S8a). As exprected, this purified bispecific
247 antibody demonstrated the ability to bind to both NK cells and RIFIN#1-expressing
248 K562 cells in flow cytometry analysis (Fig. S8b-c).
249
250 **NK-biAb exhibits an enhanced ability to trigger NK92 cytotoxicity against**
251 **RIFIN#1-expressing K562 cells.**
252 Finally, we evaluated the effect of NK-biAb on NK cell cytotoxicity against
253 RIFIN#1-expressing K562 cells. As shown in figure, the ability of this bispecific
254 antibody to trigger NK cytotoxicity was significantly enhanced compared to the
255 monospecific antibody D1D2.v-IgG. When treatment with NK-biAb at a concentration
256 of 100 nM, there was a remarkable enhancement in cytotoxic efficiency from 13.8% to
257 26.1% and from 61%-93.6%, at E/T ratios of 2.5 and 12.5 respectively, compared to
258 treatment with D1D2.v-IgG under the same conditions (Fig. 5c). Compared with
259 D1D2.v-IgG treatment, NK92 cells secreted more perforin and granzyme B in the
260 presence of 50 nM and 100 nM NK-biAb (Fig. 5d-5e). Flow cytometry results also
261 verified that NK-biAb can potently stimulate NK-cell cytotoxicity against RIFIN#1-
262 expressing K562 cells (Fig. 5f).
263

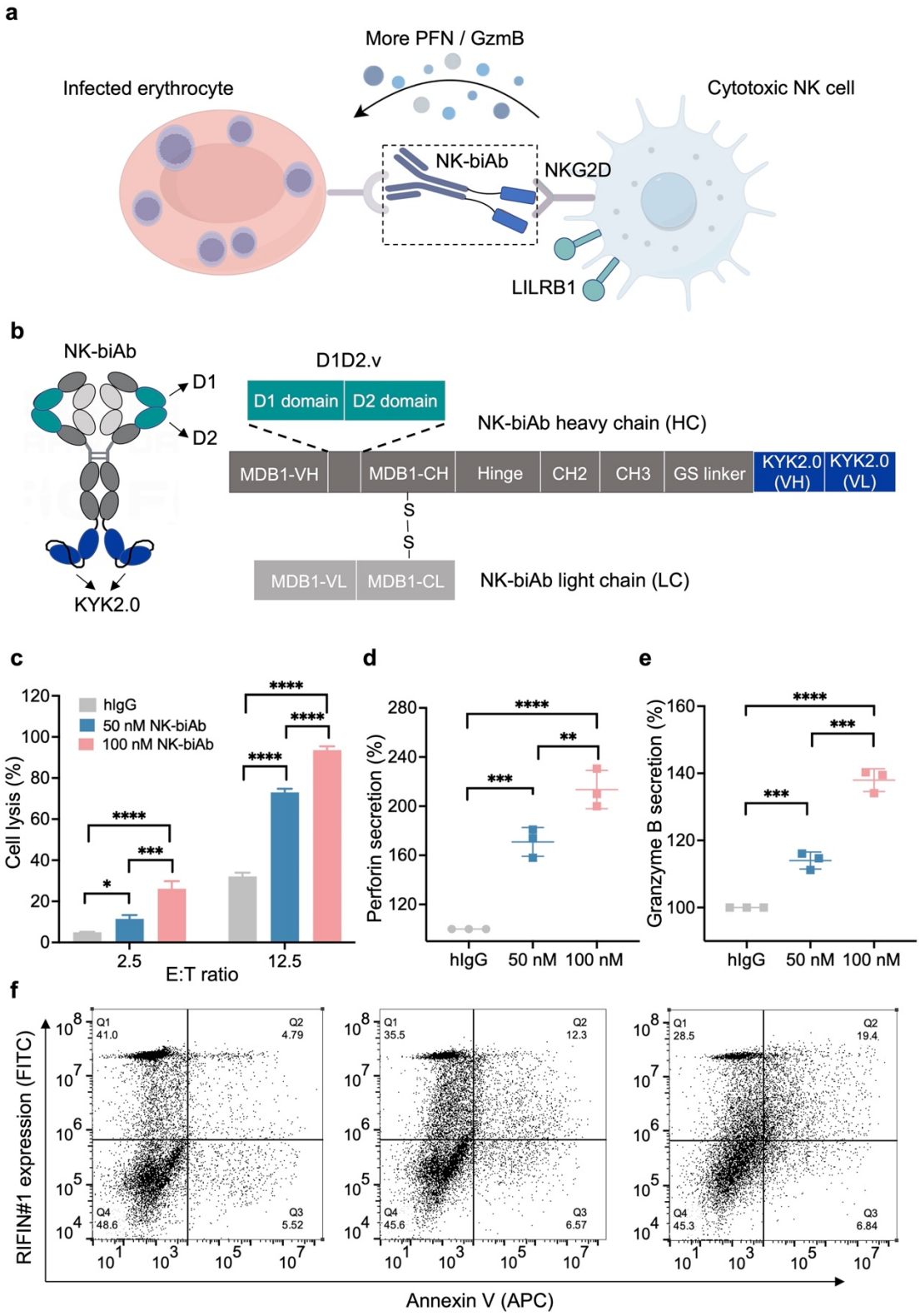

Fig. 5: Design and characterization of NK-biAb

(a) Schematic of NK cell redirections by NK-biAb. Scfv form of KYK2.0 (scfv-KYK2.0), an NKG2D activating antibody was fused to C terminus of D1D2.v-IgG. When recognizing and blocking immune escape response of *P. falciparum* via D1D2.v-Fab domains, scfv-KYK2.0 domain

can also bind to NKG2D receptors, redirect NK cells to *P. falciparum* and trigger NK cell activities. scFv-KYK2.0 is colored in light orange and NKG2D receptor is depicted as a light blue dart. **(b)** cDNA frame of NK-biAb. cDNA of D1D2.v-IgG part is the same as previously described. The heavy variable chain (VH) and light variable chain (VL) of KYK2.0 depicted in orange are fused to C terminus of D1D2.v-IgG by a GS linker. (**c)** NK92 cytotoxicity assay in the presence of NK-biAb. RIFIN#1-expressing K562 cells were cocultured with NK92 cells and incubated with 100 nM control human IgG (hIgG) or 50 nM NK-biAb (Cyan, n =3) and 100 nM NK-biAb (Red, n =3). Statistical tests were two-way ANOVA and statistical significance was analyzed between NK-biAb and hIgG. **(d,e)** Detections of the perforin (d) and granzyme B (e) releases in the presence or absence of NK-biAb. RIFIN#1-expressing K562 cells were cocultured with NK92 cells (E: T ratio = 1: 1) and incubated with 100 nM control hIgG (Grey, n = 3), 50 nM NK-biAb (Cyan, n =3) and 100 nM NK-biAb (Red, n = 3). After the incubation for 24h, the perforin and granzyme B levels were determined by ELISA. Statistical tests were one-way ANOVA and statistical significance was analyzed between NK-biAb and hIgG. **(f)** Flow detection results for the coculture of NK92 and RIFIN#1-expressing K562 for 24 h at E: T = 1: 1 in the presence of 100 nM hIgG (Left), 50 nM NK-biAb (Middle) and 100 nM NK-biAb (Right), showing the RIFIN#1-expressing K562 cells killed by NK92 cells. The data in the second quadrant stands for the lysed RIFIN#1-expressing K562 cells. *P<0.05; **P<0.01; ***P<0.001; ****P<0.0001.

Discussion

Upon infection, *P. falciparum* utilizes variant surface antigens to engage with receptors on the human host, thereby facilitating immune evasion and ensuring their survival in the host[7,8]. Recent studies have identified several receptor-containing antibodies in malaria-exposed individuals that block surface antigen-receptor interactions. Functional studies have shown that these antibodies hold potential as therapeutic agents and for incorporation into malaria vaccine design[15-17]. For instance, MGD21 antibody has been shown to promote NK cell-dependent cleavage of IEs and to inhibit the growth of *P. falciparum*[17]. However, reported receptor-containing antibodies only have either LAIR1 domain or LILRB1-D3D4 domains, and no antibodies containing LILRB1-D1D2 domains have been discovered. The RIFIN family is divided into different species, some of which interact with LILRB1-D1D2 domains rather than LILRB1-D3D4 domain or LAIR1 to transduce immunoinhibitory

signals. Therefore, the use of LILRB1 D1D2-containing antibodies for the treatment of malaria is of great importance.

In this study, we propose an in vitro strategy for designing novel receptor-containing antibodies. Our approach utilizes structure-guided affinity maturation to obtain receptor fragment variants with enhanced binding capacity, while using the framework of a human natural antibody against malaria as a template for antibody generation[15]. Due to the weak affinity between RIFIN and LILRB1-D1D2, no relevant D1D2-containing antibody has been reported. We used this strategy to artificially create high-affinity D1D2-containing antibodies, filling a gap in this field. As an illustrative example, we successfully prepared D1D2.v-IgG antibody, which has 110-fold higher affinity towards RIFIN1# than LILRB1 and can effectively block the interaction between RIFIN1# and LILRB1. Cellular experiments demonstrated that D1D2.v-IgG significantly enhanced NK cell-mediated cytotoxicity against K562 cells expressing RIFIN#1. In addition, on the basis of D1D2.v-IgG, we developed a bispecific antibody targeting both RIFIN#1 and the NKG2D receptor, which showed enhanced ability to trigger NK cell-mediated cytotoxicity compared to D1D2.v-IgG. Bispecific antibodies have been shown to be a promising avenue for immunotherapeutic interventions in a variety of malignancies[21,22,24,26]. Our data emphasize the potential application of these agents in combating malaria.

In conclusion, our study provides a strategy for the design of receptor-containing antibodies, offering potential applications in the development of malaria therapeutics and vaccines. The increasing availability of resolved structures of Plasmodium surface antigens binding to host receptors[9,11,15,17] will facilitates the development of corresponding antibodies using our strategy.

330 **Materials and Methods**

331 **Antigen purifications**

332 The variable region of RIFIN#1 (PF3D7_1254800, 165-274 aa) with an N-
333 terminal 6×His tag was cloned into a pET28a vector. The recombinant vector was
334 transformed into E.coli BL21 (gold), and the cells were induced with 1 mM IPTG at a
335 OD_{600} of 0.7. Protein was expressed as inclusion bodies and denatured in a guanidine
336 buffer (6 M Guanidine hydrochloride, 20 mM Tris pH 8.0, and 300 mM NaCl) for 4 h.
337 The inclusion bodies were then purified by Ni-NTA affinity chromatography and eluted
338 by the guanidine buffer containing additional 500 mM imidazole. The denatured
339 inclusion bodied were retrieved by dialyzing against a buffer (20 mM Tris pH 8.0, 300
340 mM NaCl) and resolubilized in the guanidine buffer. Refolding was performed by the
341 quick dilution of inclusion bodies into a buffer (1 M L-arginine, 20 mM Tris pH 8.5,
342 100 mM NaH_2PO_4, 2 mM ethylenediaminetetraacetic acid, 0.1 mM
343 phenylmethylsulfonyl fluoride, 3 mM reduced glutathione and 0.3 mM oxidized
344 glutathione) until a final protein concentration of 0.1 mg/mL-0.2 mg/mL. The refold
345 RIFIN#1 was further polished on a Superdex 75 Increase column in a PBS (pH 7.2)
346 buffer. The ECD of human LILRB1 gene with a C-terminus His tag was cloned into a
347 pTT5 vector, and the vector was then PEI-transfected into Expi293F cells (Procell,
348 China). After a post-transfection for 96 h, the supernatant was collected and the protein
349 was purified with a Ni-NTA affinity chromatography. The purified LILRB1-ECD was
350 further exchanged into PBS (pH 7.2) buffer on a Superdex 200 Increase column.

351 For biotinylation, the RIFIN#1 and LILRB1-ECD proteins were cultured with
352 NHS-pEG12-biotin in a PBS buffer (pH 7.2). The culture reactions were quenched with
353 a Tris buffer after 8 h incubation. The free NHS-pEG12-biotin reagents were splitted
354 from the biotin-labeled proteins by a size-exclusion chromatography.

355

356 **EBY100 vector construction and LILRB1-D1D2 wild type display**

357 To avoid weird display stuff, pYD1 vector was reconstructed by fusing Agar 1/2
358 domain to the C-terminus of displayed targets. Meanwhile, the detection tags of pYD1
359 vector were replaced by a N-terminal FLAG, a C-terminal V5-tag and a C-terminal His
360 tag. D1D2 wild type was co-electroporated with a precut reconstructed pYD1, while
361 yeast cells were induced with SGCAA. The signals of RIFIN#1 binding to the displayed
362 D1D2 wild type were detected by FCM.
363
364 **Constructing the library of D1D2 variants**
365 Based on the crystal structure of RIFIN#1-LILRB1 complex, a site-directed
366 library was generated by the several rounds of overlapping PCR reactions for
367 randomizing the binding residues of LILRB1-D1D2. The randomizing primers are as
368 shown in Supplementary Table 1.The overlapping PCR reactions were conducted under
369 20 cycles. The external primers for the amplification of LILRB1-D1D2 library on a
370 large scale introduce a 70 bp homologous sequence to pYD1 vector. The LILRB1-
371 D1D2 library were co-transformed into EBY100 with a precut pYD1 vector at a
372 library/vector ratio of 3: 1. Yeast transformants were recovered in a YPD/Sorbitol broth
373 and amplified in SDCAA, resulting in a library containing 2×10^7 transformants.
374
375 **MACS selections of the naive library**
376 Transformed yeast were induced in SGCAA medium at 20°C for 48 h. For the 1st
377 round selection, 4×10^8 cells referred to as 20× library size were pellet and washed with
378 a PBE buffer (PBS pH 7.2 supplemented with 0.5% BSA). Firstly, the cells were
379 resuspended in 2 mL of the PBE buffer containing 2 μM biotinylated RIFIN that had
380 been pre-coated with Streptavidin-Alexa Fluor 647 (Invitrogen, USA), followed by an
381 incubation at 4°C for 2 h. Secondly, the stained cells were pelleted by centrifugation
382 (3500 g, 5 min) , washed twice with 2 mL PBE, and resuspended in PBE containing
383 paramagnetic anti-Alexa Fluor 647 microbeads (Miltenyi Biotech, German). Thirdly, a
384 magnetically-labeled yeast cells were enriched on LS MACS column (Miltenyi Biotech,

385 German), and the enriched yeast cells were eluted with 5-10 mL PBE. Finally, the
386 selection outputs were pellet and amplified in SDCAA for next round selection. Five
387 additional selections were performed by successively decreasing concentrations of
388 biotinylated RIFIN#1 from 1 μM to 0.02 μM. In each round selection, the yeast cells
389 were first labeled with SAV-Alexa Fluor 647 after incubating with biotinylated
390 RIFIN#1 for 2 h and washed once with PBE, then coated with 100 μL of anti-Alexa
391 Fluor 647 microbeads for 30 min and washed once, and finally separated by LS MACS
392 column.
393
394 **MACS competition selections**
395 The MACS tetramer/monomer selection outputs were further performed
396 competition selections to get ultrahigh affinity variants. The induced tetramer/monomer
397 selection outputs were cultured with 0.02 μM biotinylated RIFIN#1 at 4°C for 2 h. Then
398 the cells were pellet, washed once with PBE and competed with 1 μM unlabeled
399 RIFIN#1 for 2 h. After the competition process, the cells were stained with
400 Streptavidin-Alexa Fluor 647 and coated with anti-Alexa Fluor 647 microbeads. MACS
401 sorting was also performed using LS column. By now, the 1st round competition was
402 finished, and the competition outputs were amplified and induced for next round
403 competition selection. In the 2nd round competition selection, the competing time of
404 unlabeled RIFIN was increased to 4 h, and the final selection outputs were titrated on
405 SDCAA plates for plasmid extraction and sequencing.
406
407 **Preparation of D1D2.v-IgG**
408 D1D2.v were inserted between MDB1-VH and MDB1-CH, and cloned into pTT5
409 vector as IgG4 forms. MDB1 light chain was also cloned to pTT5 vector. The DNAs
410 of MDB1 light chains and D1D2.v-IgG heavy chains were co-transfected into
411 Expi293F cells using PEI transfection reagents. After the transfection for 96 h, the
412 culture supernatant was separated by centrifugation (4000 rpm, 10 min) and purified

413 with protein A resin. The purified D1D2.v-IgG was further polished on a Superdex 200
414 Increase column in a PBS (pH 7.4) buffer.
415
416 **Characterization of D1D2.v-IgG**
417 Protein-based ELISA assays were performed to determine the affinity of D1D2.v-
418 IgG to RIFIN#1 in comparison to that of LILRB1-ECD. First, RIFIN#1 (5 μg/mL) was
419 immobilized on 96-well ELISA plates and incubated with D1D2.v-IgG of different
420 concentrations. Then, the plates were washed with PBST for 3 times and cultured with
421 the anti-human IgG-HRP at 1: 5000 dilution. Finally, the wells were washed with PBST,
422 developed with TMB for 15 min, and quenched with 2 M HCl. The absorbance at 450
423 nm was determined by a microplate reader.
424 For the protein-competition ELISA assay, RIFIN#1 (5 μg/mL) was immobilized
425 on 96-well ELISA plates, and cocultured with D1D2.v-IgG of different concentrations
426 and a competing biotinylated LILRB1 (ECD) of 1-1.5× K_d concentration, where K_d is
427 the dissociation constant. Then the plates were washed with PBST for 3 times and
428 cultured with HRP-conjugated streptavidin at 1: 2000 dilution. The absorbance at 450
429 nm was recorded by a microplate reader.
430
431 **Purifying Fab fragment of D1D2.v-IgG and its functional validation**
432 D1D2.v-IgG was digested by His-tagged HRV-3c protease overnight and
433 subjected to a negative protein A and Ni-NTA column purification. The 5-fold excess
434 of refold RIFIN#1 were co-cultured with the Fab fragment of D1D2.v-IgG and the
435 resulting complex was further polished on a Superdex 200 Increase column. The ratio
436 of RIFIN#1 binding to the Fab fragment of D1D2.v-IgG was assessed by SDS-PAGE.
437
438 **Preparation of NK-biAb and its functional validation**
439 scFv-KYK2.0 was fused to the C-terminus of D1D2.v-IgG heavy chain to generate
440 NK-biAb (M_r = 260 kDa). The DNAs of MDB1 light chains and NK-biAb heavy chains

441 were co-transfected into Expi293F cells using PEI transfection reagents. After the
442 transfection for 96 h, the culture supernatant was collected by centrifugation (4000 rpm,
443 10 min) and purified on a protein A column. The purified protein was further polished
444 on a Superdex 200 Increase column in a PBS (pH 7.4) buffer. To validate the functions
445 of NK-biAb to attach NK92 cells and bind NKG2D, the NK92 cells pre-stimulated with
446 IL-2 were cultured with NK-biAb at 37°C for 2 h, and stained with anti-human IgG-PE
447 for the detection of surface NKG2D.
448
449 **Stable RIFIN#1-expressing K562 cell line production**
450 K562 cells (Procell, China) were cultured at 37°C in DMEM with 10% FBS and
451 5% CO_2. The cDNA of RIFIN#1 with its natural signal peptide was cloned into pLVX-
452 ZsGreen plasmid. Lentivirus were produced by HEK-293T (Procell, China) for
453 infecting K562 cells. The infected K562 cells were enriched by the selection using 1
454 μg/mL puromycin, to obtain the stable RIFIN#1-expressing K562 cell line.
455
456 **Evaluation of NK cell cytotoxicity**
457 The RIFIN#1-expressing K562 cells were incubated at 37°C for 1 h with D1D2.v-
458 IgG or NK-biAb. The NK92 cells in the same volume as RIFIN#1-expressing K562
459 cells were then cocultured for 4 h at 37°C and 5% CO_2 with the incubated RIFIN#1-
460 expressing K562 cells at the E: T ratios of 2.5: 1 and 12.5: 1. The final mixtures contain
461 either 100 nM D1D2.v-IgG or 50 nM/100 nM NK-biAb. The killing efficiency (E) was
462 calculated from the absorbance (A) of CCK8 at 450 nm: $E\% = [1-(A_S-A_{EC})/A_{TC}]\times 100\%$,
463 where A_S is for the mixture of effector and target cells, and A_{EC} and A_{TC} are, respectively,
464 for effector cells and target cells.
465
466 **Cytokine measurement and FCM detection**
467 10^5 NK92 cells were cocultured for 24 h with 10^5 RIFIN#1-expressing K562 cells
468 in a 96-well plate in the presence of either 100 nM D1D2.v-IgG or 50 nM/100 nM NK-

469 biAb. Perforin and granzyme B release were detected from the supernatants of the
470 cocultured mixture by protein-based ELISA assay kits (Beyotime, China). The mixtures
471 of NK92 and K562-RIFIN#1 cells were stained for 1 h at 4°C (controlled by ice) with
472 Annexin V-APC in 100 μL PBS containing 0.5% BSA. The stained cells were detected
473 by flow cytometry, with the data analyzed by Flowjo software.
474
475
476
477 **References**

478 1. World Malaria Report 2023 [M]. World Health Organization (2023).
479 2. Burton, D. R. Antibodies, viruses and vaccines. *Nature Reviews Immunology* 2, 706-
480 713 (2002).
481 3. Haldar, K., Bhattacharjee, S. & Safeukui, I. Drug resistance in *Plasmodium*. *Nature*
482 *Reviews Microbiology* 16, 156-170 (2018).
483 4. Burton, D. R. What Are the Most Powerful Immunogen Design Vaccine Strategies?
484 Reverse Vaccinology 2.0 Shows Great Promise. *Cold Spring Harb Perspects in Biology*
485 9 (2017).
486 5. Wells, T. & Donini, C. Monoclonal Antibodies for Malaria. *New England Journal of*
487 *Medicine* 387, 462-465 (2022).
488 6. Nilsson, S. K., Childs, L. M., Buckee, C. & Marti, M. Targeting Human Transmission
489 Biology for Malaria Elimination. *PLOS Pathogens* 11, e1004871 (2015).
490 7. Sakoguchi, A. & Arase, H. Mechanisms for Host Immune Evasion Mediated by
491 *Plasmodium falciparum*-Infected Erythrocyte Surface Antigens. *Frontiers in*
492 *Immunology* 13 (2022).
493 8. Chan, J. A., Fowkes, F. J. & Beeson, J. G. Surface antigens of *Plasmodium*
494 *falciparum*-infected erythrocytes as immune targets and malaria vaccine candidates.
495 *Cellular and Molecular Life Science* 71, 3633-3657 (2014).

496 9. Harrison, T. E. *et al.* Structural basis for RIFIN-mediated activation of LILRB1 in
497 malaria. *Nature* 587, 309-312 (2020).
498 10. Saito, F. *et al.* Immune evasion of *Plasmodium falciparum* by RIFIN via inhibitory
499 receptors. *Nature* 552, 101-105 (2017).
500 11. Xie, Y. *et al.* Structural basis of malarial parasite RIFIN-mediated immune escape
501 against LAIR1. *Cell Reports* 36, 109600 (2021).
502 12. Willcox, B. E., Thomas, L. M. & Bjorkman, P. J. Crystal structure of HLA-A2
503 bound to LIR-1, a host and viral major histocompatibility complex receptor. *Nature*
504 *Immunology* 4, 913-919 (2003).
505 13. Wahl, I. & Wardemann, H. How to induce protective humoral immunity against
506 *Plasmodium falciparum* circumsporozoite protein. *Journal of Experimental Medicine*
507 219 (2022).
508 14. Cockburn, I. A. & Seder, R. A. Malaria prevention: from immunological concepts
509 to effective vaccines and protective antibodies. *Nature Immunology* 19, 1199-1211
510 (2018).
511 15. Chen, Y. *et al.* Structural basis of malaria RIFIN binding by LILRB1-containing
512 antibodies. *Nature* 592, 639-643 (2021).
513 16. Tan, J. *et al.* A LAIR1 insertion generates broadly reactive antibodies against
514 malaria variant antigens. *Nature* 529, 105-109 (2016).
515 17. Xu, K. *et al.* Structural basis of LAIR1 targeting by polymorphic *Plasmodium*
516 RIFINs. *Nature Communications* 12, 4226 (2021).
517 18. Chao, G. *et al.* Isolating and engineering human antibodies using yeast surface
518 display. *Nature Protocols* 1, 755-768 (2006).
519 19. Weiskopf, K. *et al.* Engineered SIRPα variants as immunotherapeutic adjuvants to
520 anticancer antibodies. *Science* 341, 88-91 (2013).
521 20. Gonzalez-Perez, D. *et al.* Affinity-matured DLL4 ligands as broad-spectrum
522 modulators of Notch signaling. *Nature Chemical Biology* 19, 9-17 (2023).

523 21. Kwong, K. Y. *et al*. Generation, affinity maturation, and characterization of a
524 human anti-human NKG2D monoclonal antibody with dual antagonistic and agonistic
525 activity. *Journal of Molecular Biology* 384, 1143-1156 (2008).
526 22. Zhang, C. *et al.* Bispecific antibody-mediated redirection of NKG2D-CAR natural
527 killer cells facilitates dual targeting and enhances antitumor activity. *The Journal for*
528 *Immunotherapy of Cancer* 9 (2021).
529 23. Zhao, C. *et al.* A new approach to produce IgG (4)-like bispecific antibodies. *Scitific*
530 *Reports* 11, 18630 (2021).
531 24. Wolf, N. K., Kissiov, D. U. & Raulet, D. H. Roles of natural killer cells in immunity
532 to cancer, and applications to immunotherapy. *Nature Reviews Immunology* 23, 90-105
533 (2023).
534 25. Albinger, N., Hartmann, J. & Ullrich, E. Current status and perspective of CAR-T
535 and CAR-NK cell therapy trials in Germany. *Gene Therapy* 28, 513-527 (2021).
536 26. Leaver-Fay, A. *et al.* Computationally Designed Bispecific Antibodies using
537 Negative State Repertoires. *Structure* 24, 641-651 (2016).
538
539 **Acknowledgements:** Funding was provided by the National Key R&D Program of
540 China (Grant No. 2023YFA1607500), the National Natural Science Foundation of
541 China (Grant No. 32371362), and the Anhui Major Basic Research Projects (Grant No.
542 2023z04020016).
543
544 **Author contributions:** Y.W and H.T contributed equally to this work. Y.W initiated
545 the project, performed the library construction and selections, prepared antigen samples
546 and performed biochemical assays. H.T performed the FCM detections and conducted
547 the stable cell line production, cytotoxicity assays and ELISA assays. W.W performed
548 the antibody purifications and functional validations. L.M helped to prepare
549 biotinylated sample preparations. C.Z helped to perform biochemical assays and FCM
550 detections. Y.W. and B.W analyzed the data, interpreted the results. J.W, H.D and B.W

prepared the manuscript. J.W., B.W and H.Z supervised the project. All authors read and edited the manuscript.

Competing interests: The authors declare no competing interests.

Data and materials availability: All data and materials are available within the paper and its supplementary materials. Extra data are available from the corresponding author (J. Wang) upon reasonable request.

List of Supplementary Materials

Fig S1 to S8 for multiple supplementary figures

Table S1 for supplementary table